Experimental Thermal and Fluid Science 146 (2023) 110926

Contents lists available at ScienceDirect

Experimental Thermal and Fluid Science

journal homepage: www.elsevier.com/locate/etfs

Cavitation induced by pulsed and continuous-wave fiber lasers in confinement

Jelle J. Schoppink [a,*], Jan Krizek [b], Christophe Moser [b], David Fernandez Rivas [a]

[a] Mesoscale Chemical Systems group, MESA+ Institute and Faculty of Science and Technology, University of Twente, P.O. Box 217, 7500 AE Enschede, The Netherlands

[b] Laboratory of Applied Photonics Devices, École Polytechnique Fédérale de Lausanne (EPFL), Station 17, 1015 Lausanne, Switzerland

ARTICLE INFO

Keywords:
Vapor bubble
Cavitation
Pulsed laser
CW laser
Jet injection
Thermocavitation
Microfluidic confinement

ABSTRACT

Bubbles generated with lasers in liquids under confinement have been investigated for their potential use as the driving mechanism for liquid micro-jets in various microfluidic devices, such as needle-free jet injectors. Here, we report on the study of bubble formation by a continuous-wave (CW) and a pulsed laser inside an open-ended microfluidic capillary. This results in a direct comparison between bubbles generated by laser sources emitting light in different time scales (ms and ns). The bubble kinetics represents an important parameter because it determines the available kinetic energy for a subsequent liquid jet.

We show that the bubble growth rate increases linearly with the delivered energy for both the CW and the pulsed laser. Experiments show that at equal absorption coefficient, the bubble growth for both lasers is similar, which indicates that they can be used interchangeably for jet generation purposes. However, bubbles generated by a CW laser require more optical energy, which is due to heat dissipation. Furthermore, the bubbles generated by the CW laser show a slightly larger variation in size and growth rate for identical initial conditions, which we attribute to the stochastic nature of thermocavitation.

1. Introduction

Laser cavitation is widely used for medical applications [1], including ablation of biological tissue [2], bioprinting [3], sonoporation of cells [4] and lithotripsy [5,6]. Lately, lasers have also been investigated for their use in laser-actuated needle-free jet injectors (NFJIs) [7]. These NFJIs present many advantages over conventional hypodermic needles, such as improved patient compliance [8], reduction in needle waste [9], improved safety for healthcare workers [10], injection of high-viscous liquids [11] and better control over injection parameters [7,12].

The working principle of these laser-actuated NFJIs is similar to that of laser-induced forward transfer, where a laser is heating a liquid resulting in the formation of a vapor bubble [13,14]. For NFJIs, the liquid is contained in an open-ended microfluidic channel, such that the explosively growing bubble pushes the liquid through a small opening, which results in the formation of a fast microfluidic jet with the ability to penetrate the skin. Jet velocities can be controlled by the delivered energy [15], optical beam size [16], channel geometry [15,17] or the inclusion of a tapered nozzle [18]. The jet velocity affects the type of impact on substrates [19] and is linearly proportional to the injection depth [16], a dependence that allows to target specific skin layers.

NFJIs can be actuated by a pulsed laser [15,16,20–23], or a continuous-wave (CW) laser [17,18,24,25]. Although both laser types can create jets able to penetrate skin-like substrates, a comparison between the two methods is difficult, as all studies use different injector geometries, laser configurations, ejected liquid volumes and disparate substrates for injection [7]. The difference between the two laser types is in the time of irradiation and bubble formation dynamics, as shown in Fig. 1.

For the pulsed laser, the bubble forms shortly after the ns pulse with very high peak power ($\gtrsim 0.5-2$ GW/cm^2). The laser–liquid interaction of pulsed lasers has been investigated thoroughly by, among others, Vogel et al. This work focused on the optical breakdown and plasma formation at high energy densities [26], the bubble collapse [27] and resulting shock wave emission [28,29] and laser-ablation of tissue [2]. However, most recent work on pulsed-laser actuated jetting relies on linear absorption of low-pulse energies ($F < 20$ J/cm^2 [16]), below the optical breakdown threshold of approximately 500 J/cm^2 [26]. In

* Corresponding author.
E-mail address: j.j.schoppink@utwente.nl (J.J. Schoppink).

https://doi.org/10.1016/j.expthermflusci.2023.110926
Received 24 November 2022; Received in revised form 20 February 2023; Accepted 9 April 2023
Available online 13 April 2023

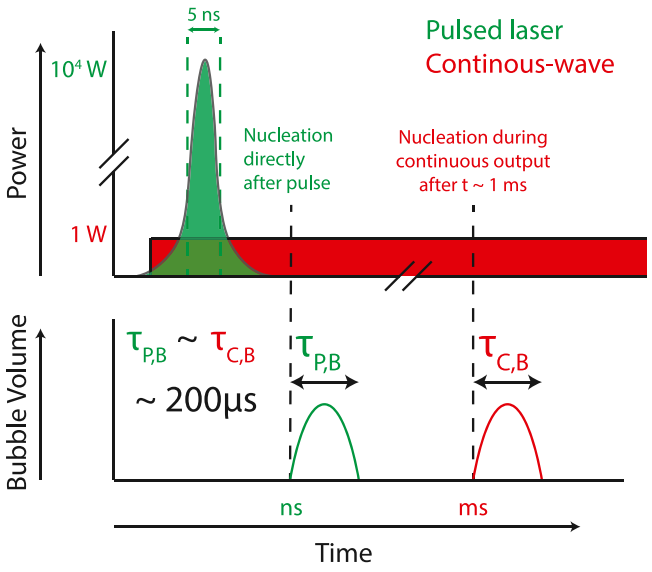

Fig. 1. Schematics indicating the main difference between the timescale of nucleation and power for the pulsed and continuous-wave laser. For the pulsed laser (green), all energy is delivered with a high peak power within 5 ns, after which nucleation occurs and the bubble forms. For the continuous-wave laser (red), the power is switched on and remains working continuously at low power. After some time during this laser illumination ($\tau \sim$ ms, depending on the power), bubble nucleation occurs. Although the timescales are different, the bubbles show similar dynamics and lifetimes ($\tau_{P,B} \sim \tau_{C,B} \sim 200$ µs).

this regime, the maximum size of a bubble formed on a solid surface increases proportionally to laser fluence [3].

In the case of CW, the laser irradiates continuously and therefore, heats the liquid slower (ms). At a certain time after the beginning of radiation ($\tau_C \sim$ ms), there is enough energy for nucleation and subsequently, the bubble forms. Bubbles formed by high-power CW or free-running Holmium lasers (P ~ 1 kW) have been investigated by Delacretez, Asshauer and others [30–33]. These floor-standing Holmium lasers irradiate at 2.12 µm for 100-1000 µs. Due to the high absorption coefficient of water at this wavelength, the liquid is heated up through linear absorption, resulting in bubble formation after approximately 50 µs [32]. Similar to the early work on pulsed lasers, their focus was on laser-ablation of tissue and bubble acoustics; though the exact bubble dynamics were not reported in detail. More recently, interest shifted towards more affordable and compact low-power CW lasers, with typical powers of 0.1–5 W. In this regime, the bubble size can be increased by delaying the moment of nucleation [34], through a reduction of power [34] and/or absorption coefficient [35,36] or an increase in beam size [37].

In this manuscript, we investigate laser-actuated cavitation at a fiber tip in an open capillary, and we compare two types of lasers, the ns-pulsed and the CW laser. This comparison provides a better understanding of the energy transfer from the optical energy into the kinetic energy, which is of great importance for the use of laser-actuated cavitation in needle-free jet injectors.

2. Theory

Fig. 1 shows the difference in timescales between nucleation by the pulsed (ns) and CW lasers (ms). The difference in timescale has an effect on three parameters: the absorption of the optical energy, thermal diffusion and potential pressure confinement. These will be explained below.

First of all, the energy absorption by the liquid can be split up into two categories: linear and non-linear. The former depends on the absorption coefficient α of the liquid at the laser wavelength. As linear absorption does not depend on timescale, it is present in both pulsed and CW laser exposition. In the case of only linear absorption, the optical penetration can be calculated by [38]

$$\Psi(z) = \Psi_0 \exp(-\alpha z), \tag{1}$$

where Ψ is the laser irradiance, Ψ_0 is the incident irradiance, and z is the position along the laser beam. Therefore, a typical penetration depth $d = \frac{1}{\alpha}$ can be defined, at which the irradiance has dropped to $\Psi(d) = \exp(-1)\Psi_0 \approx 0.37\Psi_0$, which means that approximately 63% has been absorbed. As linear absorption of water is negligible in the visible and near-infrared ($\lambda < 1300$ nm) [39], a dye is typically added to increase the absorption [34]. Non-linear absorption may occur at sufficient power densities, which is a result of optical or thermal breakdown [2]. The threshold for this optical breakdown is found to be around 10^{-11} W/m^2 or ~ 500 J/cm^2 for laser pulses of 6 ns at a wavelength of 1064 nm [26]. However, the threshold is reduced up to three orders of magnitude when the target has a very high linear absorption coefficient [2]. Beyond this threshold, it was found that the bubble increases linearly with increasing pulse energy [26].

Secondly, thermal diffusion plays a significant role when the timescale of nucleation is comparable to the thermal diffusion timescale. The thermal diffusion time t_d is given as [40]

$$t_d = \frac{\delta^2}{4\kappa}, \tag{2}$$

where κ is the thermal diffusivity of the liquid, and δ is the typical length scale, which is either the beam diameter or the typical absorption length, whichever is smaller. In the case of heating water ($\kappa \approx 0.14$ mm^2/s) with a beam diameter of 50 µm and absorption length of 100 µ m, the thermal diffusion time (over the length of the beam diameter) is approximately 4 ms. Therefore, thermal diffusion does not play a role in the pulsed laser actuation ($\tau_{pulsed} \sim$ ns), but does influence the CW actuation ($\tau_{cw} \sim$ ms). For CW cavitation, a decrease in laser power or increase in beam size delays nucleation, and results in more heat dissipation. It then requires more energy to reach the nucleation temperature, and produces larger bubbles [34].

However, in the case of pulsed laser-generated pulsed bubbles, heat transfer across the bubble–liquid interface does influence the bubble dynamics. Sun et al. found that the inclusion of heat transfer is required for a numerical model of the growth and collapse of the bubble in a microcapillary [41]. However, due to short bubble lifetimes in the order of 200 µs, typical heat diffusion length scale is 10 µm (using Eq. (2)). Consequently, heat transfer occurs primarily near the bubble surface, which affects further evaporation/condensation. Sun et al. further explained that the heat exchange with the channel wall could be neglected. They also found that the bubble collapse is slower than the growth in microchannels, and such an effect increases with smaller channel sizes.

Third of all, the rapid heating of the liquid results in thermoelastic stresses in the irradiated volume, as the system tends to reconfigure to a new equilibrium [2]. Pressure confinement may play an important role in defining the threshold for liquid–gas transition [42]. In the case of irradiation from an optical fiber, the finite size of the fiber enhances this effect [42]. When this heating is sufficiently fast, the pressure is confined within the irradiation volume near the fiber tip. The time for a pressure wave to travel across the irradiated volume is [43]

$$t_p = \frac{\delta}{c_{\text{water}}}, \tag{3}$$

where c_{water} is the speed of sound in water (1480 m/s). For a fiber diameter of 50 µm and absorption length of 100 µm, $t_p \approx 34$ ns. This means that for pulsed laser actuation, the pressure is mostly confined to the region close to the fiber. In the absence of pressure confinement (when the laser pulse duration is much longer than t_p), there is significant thermal expansion of the heated volume during the irradiation. Therefore, the thermoelastic stresses are reduced, and the built-up pressure at bubble formation is reduced [2].

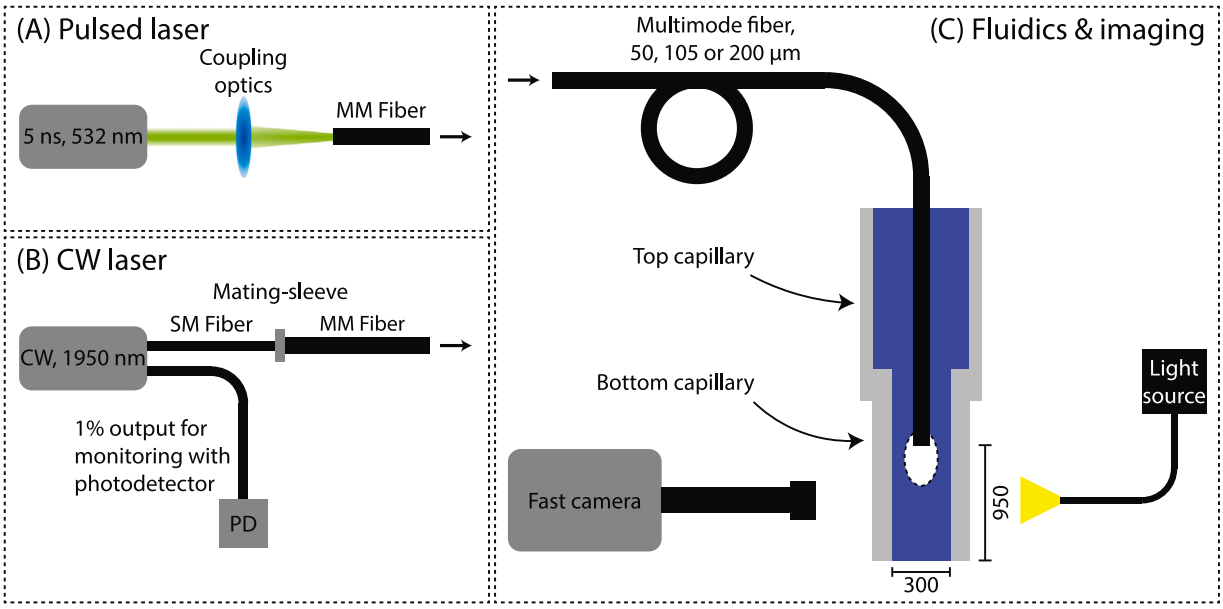

Fig. 2. Experimental setups consisting of a laser, either pulsed (A) or continuous-wave (B), coupled into a multimode optical fiber, which is inserted into a capillary system (C). A high-speed camera (Photron NOVA S6), together with a light source (Schott CV-LS), is used for imaging. The inner diameter of the smaller capillary is 300 µm, and the distance between the fiber tip and the liquid–air interface is 950 µm. Due to the smaller inner diameter of the lower capillary compared to the upper capillary (ID = 1200 µm), surface tension ensures that the lower capillary will constantly be filled after each jet generation.

3. Experimental methods

Fig. 2 shows the experimental setups, which consist of a fiber-coupled laser and a microfluidic capillary system. Two laser types are used, a pulsed and a CW laser. For all the experiments, the laser is coupled into a multimode optical fiber with core diameter varying from 50, 105 and 200 µm (Thorlabs FG050LGA, FG105LCA, FG200LEA). This fiber is inserted into a capillary system filled with water. Upon laser illumination, a bubble forms at the laser tip.

The pulsed laser (Continuum, ML-II) has a pulse duration of 5 ns and a wavelength of 532 nm. The laser light is coupled into the optical fiber using a two-mirror system and a focusing objective. Before and after each experiment, the pulse energy at the output of the optical fiber is measured using an energy sensor (Thorlabs ES111C). The light energy coupled into the fiber varied between 50 and 700 µJ. For the 50 and 105 µm fiber the upper pulse energy limit was approximately 130 and 480 µJ due to the laser-induced damage threshold for the fiber tip.

The CW laser (BKTel Photonics, HPFL-2-350-FCAPC) has a wavelength of 1950 nm, which was deliberately chosen to match the absorption peak of water ($\alpha \approx 12000$ m^{-1} [39]). The output power can be varied from 0.2 to 3 W. The laser is initially coupled into a single-mode fiber (Corning SMF-28e), which is then connected through a mating sleeve to the respective multimode fiber. The laser also has a secondary fiber output at 1% of the nominal power, which is connected to a photodetector (Thorlabs DET05D2) to monitor the output power using an oscilloscope (Tektronix MSO2014B).

The multimode fiber is inserted into a capillary system, which consists of two concentric connected capillaries with inner diameters of 1500 (top) and 300 µm (bottom). Initially, the capillary system is completely filled with water, and capillary flow from the larger to the smaller capillary ensures that the 300 µm capillary will be completely filled. The fiber is inserted partially into the 300 µm (bottom) capillary and has a distance of 950 µm to the end of the capillary (the liquid–air interface).

For the experiments with the 532 nm laser and 105 µm fiber, we increased the absorption with aqueous solutions of Allura Red AC (ARAC, red food dye) with varying concentrations between 5 and 52 mM. The absorption coefficients were measured and compared with values reported in the literature (see Appendix A). The surface tension was measured using the pendant droplet method [44], and we found that the dye slightly reduces the surface tension to 65 ± 2 mN/m for the largest concentration (52 mM), compared to 71 mN/m for pure water. The viscosity was measured using a Anton Paar MCR 301 rheometer, with parallel plate configuration. The dye did not affect the viscosity, which was 1 mPa s, irrespective of the dye concentration. For the 50 and 200 µm fiber, only the 10 mM (≈ 12000 m^{-1}) and 52 mM (≈ 19000 m^{-1}) were used. The 10 mM was chosen as the absorption coefficient matches the absorption coefficient of the CW laser experiment in this study, and the 52 mM was chosen as it was used in previous studies [16,45].

A Photron NOVA S6 high-speed camera was used in combination with Navitar 12x zoom lens system and a Schott CV-LS light source for visualization of the bubble dynamics. The camera is used at a framerate of 192k fps, a resolution of 256*80 and a pixel size of 5 µm. Fig. 3 shows a few typical images during the bubble lifetime. The images are analyzed with a custom-made MATLAB algorithm, which tracks the bubble over time, and calculates the volume assuming cylindrical symmetry. The average growth rate is calculated as the maximum bubble size divided by the growth time.

4. Results and discussion

4.1. Pulsed laser

Bubble volume and volumetric growth rate

Fig. 3(a) shows typical experimental images of the bubble generated by the pulsed laser (more examples in Appendix B). The bubble appears at the fiber tip and grows towards the free surface until it reaches a maximum size and collapses. Occasionally, cavitation bubbles inside the bulk liquid appear due to the negative peak pressure of the shock wave within a few frames after the laser pulse ($\tau < 20$ µs). As these cavitation bubbles remain small (R < 10 µm) and do not affect the main bubble or the jet, we will not discuss them further. These bubbles are further discussed in Ref. [46].

The calculated bubble volume over time is shown in Fig. 3(b). We can observe parabolic-like behavior, although the growth is typically slightly faster than the collapse ($\approx 5-20\%$), which was also observed by Sun et al. both numerically as well as experimentally [41]. From

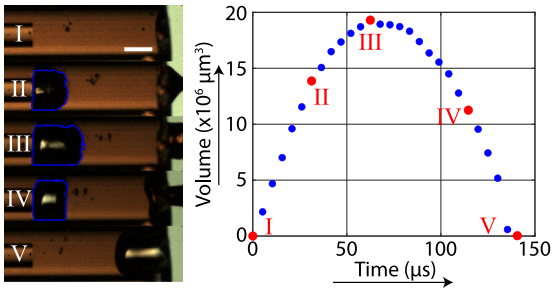

Fig. 3. Bubble volume over time for an experiment with the pulsed laser (d_{fiber} = 105 µm, dye concentration C_{ARAC} = 10 mM, E_{pulse} = 233 µJ). **Left:** Five images during the experiment, with the tracked bubble in blue. Respectively: just before the laser pulse, during the growth phase, at maximum volume, during the collapse, and after the experiment showing the expelled volume. The white scale bar in the top figure measures 200 µm. **Right:** Bubble volume plotted versus time dependence, the red dots corresponds to the 5 images on the left (I–V)..

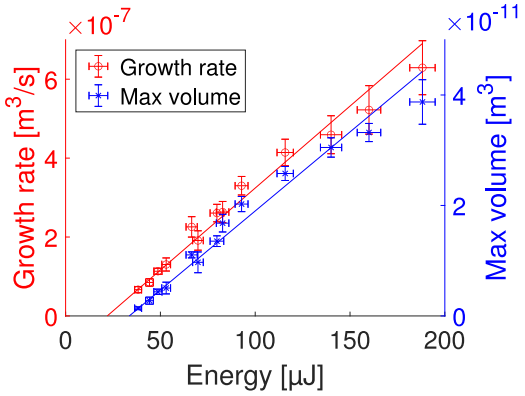

Fig. 4. Maximum bubble volume (blue, right axis) and average volumetric growth rate (red, left axis) for a range of pulse energies with the 105 µm fiber and 52 mM dye concentration. Each data point is an average of at least 6 individual measurements with the error bars indicating standard deviation. Solid lines indicate a linear fit for both variables.

the bubble volume curve, the average growth rate is calculated by the maximum size divided by the growth time.

Fig. 4 shows the maximum bubble volume and average volumetric growth rate for a range of laser pulse energies. Both the volume and the growth rate show a linear behavior with the pulse energy, meaning that it is a good indication of the jet velocity, which also increases linearly with pulse energy [16]. In this previous study, it was confirmed that the jet velocity grows linearly with laser energy using the same range of energies, resulting in velocities 0–125 m/s [16] and using a dye concentration of (52 mM ARAC).

Interestingly, the offset of the fit, which can be seen as the threshold energy for bubble formation, is not equal for both fits. Therefore, extrapolating this linear relation would indicate that bubbles with zero volume still have a positive growth rate, which would not be possible. We attribute this to the fact that for these very small bubbles, there are errors in bubble detection due to their small size and their short lifetime. These smallest bubbles typically only span 10 by 20 pixels in the image and have a bubble lifetime of approximately 40 µs. Thus, the growth time is only ~20 µs, which is 4 frames. This means that the actual maximum bubble size may actually be reached between two frames and not captured by the camera. Therefore, we think that the average growth rate is a better parameter to show the bubble dynamics as a function of pulse energy.

Dye concentration effect

The bubble growth rate as a function of the pulse energy is plotted in Fig. 5, for a range of dye concentrations and the 105 µm fiber tip.

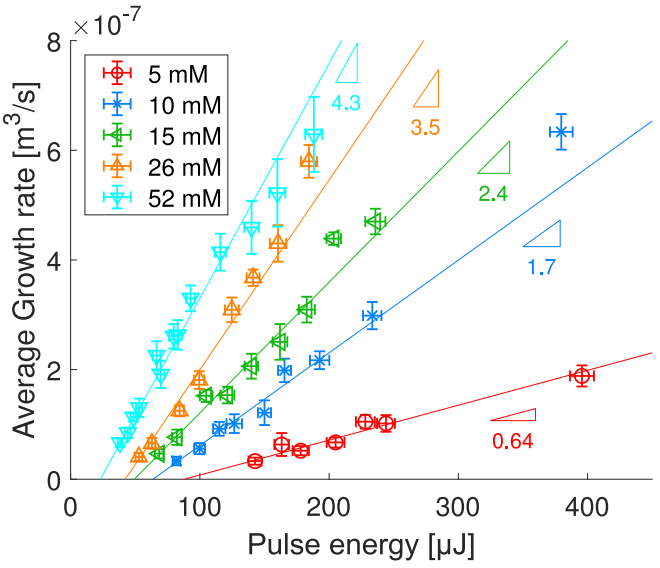

Fig. 5. Average growth rate of the bubbles generated by the pulsed laser with the 105 µm fiber for a range of pulse energies and 5 different concentrations of ARAC. Error bars indicate standard deviation in pulse energies and bubble growth rate for at least 6 individual bubbles with identical initial conditions. For each concentration, the data is fitted with a linear fit, with corresponding slope (units of 10^{-9} $m^3/(s*\mu J)$).

For all pulse energies, an increase in dye concentration results in a larger growth rate. This is explained by the fact that an increasing dye concentration increases the absorption coefficient and thus a more localized energy absorption. This results in higher liquid temperatures and more vaporization.

These results indicate that the bubble and resulting jet dynamics can be controlled by the absorption coefficient of the liquid. This means that a jet injector relying on a pulsed laser is not limited by the range of pulse energies, as an increase or decrease in dye concentration will result in a change in jet velocity and injection depth. Furthermore, by increasing the dye concentration, the required pulse energies will decrease, which would allow the use of lasers to be more affordable and possibly smaller in size.

More specifically, the absorption coefficients we used of 0.7–2 × 10^4 m^{-1} are similar to the absorption coefficients of water around its peak at 2 µm [39]. Holmium and Thulium lasers operate near this absorption peak and are often used for the irradiation of water and biological tissues [47]. Larger absorption coefficients have been used, either by employing a different dye [15], or by using an Er:YAG laser [48,49], where the absorption coefficient of water is approximately two orders of magnitude larger [50]. In the first case, even lower pulse energies (E = 19 µJ) than the ones in this study would result in a bubble and jet (although in a different setup). However, for the second case, the Er:YAG laser has a much longer pulse duration of 250 µs [38,49], for which reason there is no thermal or pressure confinement, and it operates similarly to the CW laser. Therefore this laser typically requires pulse energies 400–1000 mJ for bubble and jet formation [49,51], which is three orders of magnitude larger than used in our study. Besides that, Er:YAG lasers are not compatible with fiber delivery [5]. Near 1450 nm, there is another peak in the absorption coefficient of water, although twice as small (α = 3150 m^{-1} [39]) compared to the lower limit in our study. A previous study [52] with a 1574 nm laser ($\alpha \approx 900$ m^{-1}) showed that it would require pulse energies of 2–4 mJ, approximately one order of magnitude larger compared to the energies probed here. For even smaller wavelengths, absorption of water is negligible, and thus studies without the use of a dye rely fully on non-linear absorption and require more energy [22].

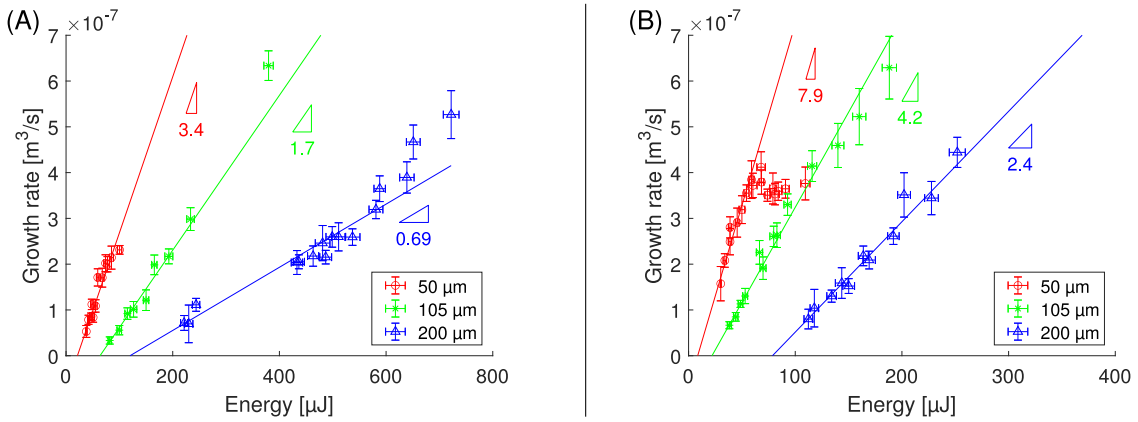

Fig. 6. Average volumetric bubble growth rate for three optical fiber sizes. Error bars indicate standard deviation of at least 6 individual measurements. Solid lines indicate the best linear fit, with corresponding slope (units of 10^{-9} $m^3/(s*\mu J)$). (A): Dye concentration of C_{dye} = 10 mM. (B): Dye concentrations of C_{dye} = 52 mM.

Fiber core diameter

Fig. 6 shows the volumetric bubble growth rates for the three different fiber core diameters: 50, 105 and 200 µm. Fig. 6A is for the ARAC concentration of 10 mM and Fig. 6B is for the ARAC concentration of 52 mM. The measurement data per fiber are fitted with the best linear fit. For both concentrations, larger fibers require larger pulse energy to obtain the same growth rate. This trend was also observed for jet velocity and fiber sizes [16], and explained by a larger energy density for the smaller fibers, and thus a larger pressure. This means that a smaller fiber with a less powerful laser can create the same bubble and resulting jet.

However, for the 50 µm fiber, we could not reach very large growth rates for two reasons: First, for the 52 mM dye concentration, we observed a plateau in the growth rate for pulse energies larger than 60 µJ. Second, the tip of the 50 µm fiber is very prone to damage — because of high light power densities, and the laser-induced damage threshold was found at approximately 120 µJ. This means that the larger fibers are more flexible in their use, although they require larger pulse energies.

Energy threshold for bubble nucleation

The intersection with the x-axis of the linear fits in Figs. 5 and 6, indicates an energy threshold for bubble formation. These energy thresholds are plotted against the irradiated volumes in Fig. 7. The irradiated volume is calculated until the typical absorption length δ, assuming a conical shape (due to divergence) starting at the fiber tip with a diameter equal to the core diameter (see Appendix C). The linear trend of the energy threshold with the irradiated volume indicates a constant energy density required for bubble nucleation. Therefore, the energy threshold scales quadratic with the fiber radius and linear with the absorption length. However, in the case where the absorption length is much larger compared to the fiber radius, the beam divergence should be taken into account. In practical applications where less powerful lasers are preferred, the fiber should have a small core radius, small NA (small divergence) and the liquid should have a large absorption coefficient.

The linear fit has a slope of 5.4×10^5 J/m^3, which would correspond to an average temperature increase in the irradiated volume of 13°C (assuming ρ = 997 kg/m^3, C_p = 4184 J/(kg °C)). Although this temperature increase seems small, it is almost equal to measured temperature increases of at most 12.8°C after pulsed laser-induced bubbles [53]. Furthermore, this is the average temperature in the irradiated volume, but the temperature of the liquid close to the fiber tip will be higher. Similarly, assuming a latent heat of water of 2260 kJ/kg, this energy density threshold is enough to vaporize approximately 2.4% of the irradiated volume.

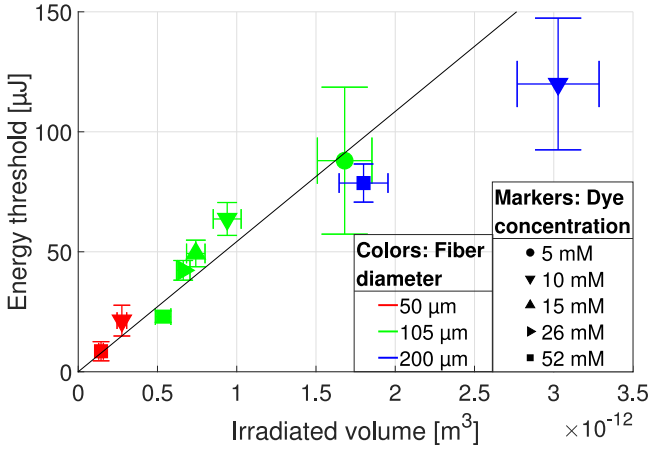

Fig. 7. Energy threshold taken from offset in the linear fits from Figs. 5 and 6, plotted against the irradiated volume. Colors indicate the different fiber diameters, symbols indicate dye concentrations and error bars indicate 95% confidence interval for the linear fits. The black line indicates the best linear fit.

This knowledge of the energy threshold may be useful for improving the computational models on laser-generated bubbles. Computational models have been used to simulate laser-generated bubbles near a free surface and the subsequent jet [18,54,55]. However, the initial bubble parameters are typically found empirically to match experimental images [18,54]. Therefore, even though this threshold value may include a systematic error due to our spatiotemporal resolution, it may help as a starting point for modeling the initial bubble parameters.

4.2. CW laser

Nucleation time and delivered energy

In contrast to the pulsed laser, for the CW experiment, only the power can be directly controlled, and not the energy. Here, the delivered energy depends on the power and the moment of nucleation, which depends on the laser power [34]. Fig. 8A shows the influence of the laser power on the nucleation time for the three fibers. First, the nucleation time increases with decreasing laser power, as it takes longer to reach the nucleation temperature. Second, for fixed laser power, the nucleation time increases with increasing fiber diameter. This is explained by an increase in beam size and thus a decrease in intensity, for which reason it takes longer to reach the nucleation temperature. Due to a limited range of laser power, sub-ms nucleation times could not be reached for the 200 µm fiber.

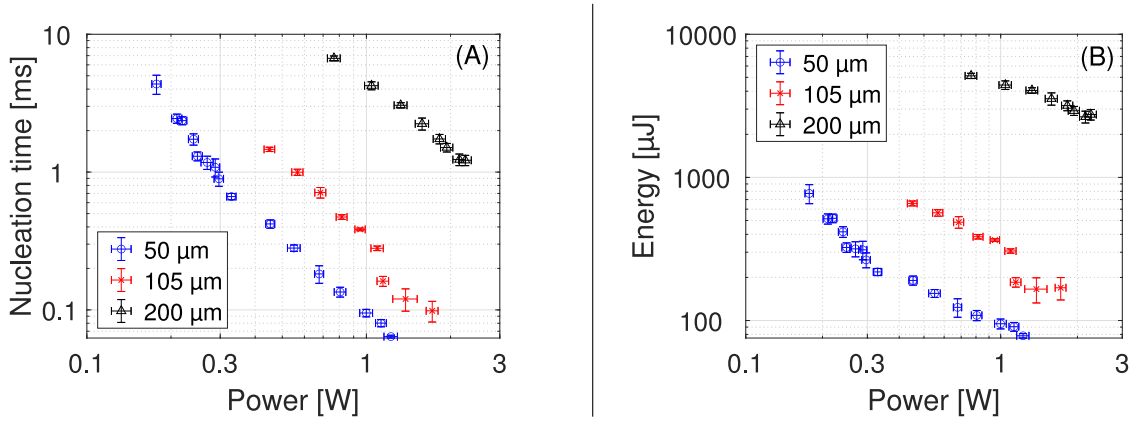

Fig. 8. Nucleation time (A) and delivered energy (B) as a function of CW laser power for three optical fibers with different diameter. Each data point is an average over at least 6 individual measurements, with the error bars indicating the standard deviation.

Besides the influence of the power and fiber size, there are fluctuations in nucleation time for each individual data point. This fluctuation in nucleation time is called *jitter* [34] and is explained by the stochastic nature of nucleation. These fluctuations linearly affect the delivered energy, and thus reduce the reproducibility. We find that the typical fluctuation (standard deviation) is approximately 8% of the nucleation time, which is smaller compared to earlier findings up to approximately 60% [34,35]. We attribute this to the fact that bubbles develop directly at the optical fiber, instead of heating a liquid with a non-collimated laser beam, where the beam size is more difficult to control and reproduce. Furthermore, in our case, we do only create individual bubbles, after which the liquid cools down again, which may result in a more reproducible nucleation time.

The delivered energies, which are calculated by multiplying the nucleation time and the power, are shown in Fig. 8B. Similar to the nucleation times, a reduction in power or an increase in fiber size results in an increase in the energy delivered. This is because an increase in nucleation time results in an increase in heat diffusion. This heat diffusion will result in an even longer nucleation time as the local temperature increase at the fiber tip is slower, which then results in larger delivered energy. For the 50 and 105 µm fibers, the CW laser results in comparable energies as the ns-laser. However, for CW the energies required for bubble formation by the 200 µm fiber are an order of magnitude larger due to the longer nucleation times, which is caused by the larger fiber area and thus lower intensities.

Previous work of Ref. [18] refers to a free-space laser diode with free-space light focusing with a 6*33 μm^2 laser beam. For a power of 0.5 W, they found a nucleation time of 600 µs, resulting in a delivered energy of 300 µJ, for a liquid with a similar absorption coefficient as ours (α = 1.0 and 1.2 * 10^4 m^{-1} respectively). The beam size for the smallest fiber in our study is already 10 times larger and still results in twice as fast nucleation time for 0.5 W (~ 300 µs). Therefore, the previous study with free-space optics and a glass microdevice showed a significant optical loss between the laser diode and the microfluidic channel. Here, due to the direct contact of the fiber and the liquid, the number of interfaces is minimized and can be no losses due to misalignment, resulting in higher energy transfer efficiency.

Bubble growth rate

The bubble growth rates for the CW laser source are shown in Fig. 9A. It is clear that the growth rates of the bubbles generated with the 200 µm fiber are much larger compared to the 50 and 105 µm fiber. The increased growth rate is explained by the delivered energy, which is an order of magnitude larger compared to the other fibers. As discussed above, smaller energies could not be delivered with the used CW laser for this fiber as it would require much larger powers. The bubbles generated at the 200 µm fiber are also much larger compared to the other two fibers, and all generated bubbles grow beyond the edge of the capillary, for which reason they coalesce with the surrounding air before reaching their maximum volume. An example of such a bubble generated at the 200 µm fiber is shown in Appendix D.

Fig. 9B shows a close-up of the growth rates of the bubbles generated at the two smaller fibers. It shows that for the CW laser, the bubble growth rate also increases linearly with increasing delivered energy. For most energies, the 50 µm fiber has a larger growth rate compared to the 105 µm fiber, which can be explained by the larger energy density. However, for delivered energies larger than 500 µJ, the 105 µm fiber results in faster-growing bubbles. We attribute it to the longer nucleation time for the 50 µm fiber to reach those levels of energy. For the 50 µm fiber, the nucleation times to reach E > 500 µJ is t_n > 2 ms, whereas for the 105 µm fiber, the nucleation time is only half. Therefore there is increased heat dissipation for the 50 µm fiber, and thus a smaller efficiency. Therefore, the growth rate no longer increases linearly with the delivered energy, and larger growth rates require much more energy for the 50 µm fiber.

Interestingly, extrapolating the linear fit of the 50 µm fiber in Fig. 9B shows a positive growth rate for zero energy, which is physically not possible. However, due to thermal dissipation, it is questionable whether the growth rate for the CW-laser would actually be linear with the energy, as thermal dissipation may reduce the energy efficiency. Therefore, even though the initial behavior for both fibers seems linear, extrapolating this to find an energy threshold does not seem to have a physical meaning.

Secondary bubbles

For small bubbles generated by the CW laser (R < 150 µm), we observe the formation of a secondary bubble at the vapor–liquid interface, see Fig. 10. These events are different from twin cavitation bubbles reported in Ref. [35], where the initial bubble first partially collapses before forming a secondary bubble. In our case, the secondary bubble typically forms when the initial bubble reaches its maximum. Furthermore, in our case, the volume of the second bubble is smaller compared to the first one, for which reason its appearance does not affect the parabolic shape of the bubble volume versus time. These secondary bubbles can be explained by the fact that the laser remains irradiating during the bubble formation and, therefore, further heats the liquid during the bubble growth. In the case of large laser powers and short nucleation times, this heating during the bubble lifetime could create a secondary bubble. In the case of Fig. 10, the growth time of the bubble takes 40 µs, whereas the initial nucleation time was 135 µs, which means that after nucleation, another 30% of the initial energy is still delivered, which results in secondary nucleation at the vapor–liquid interface of the bubble.

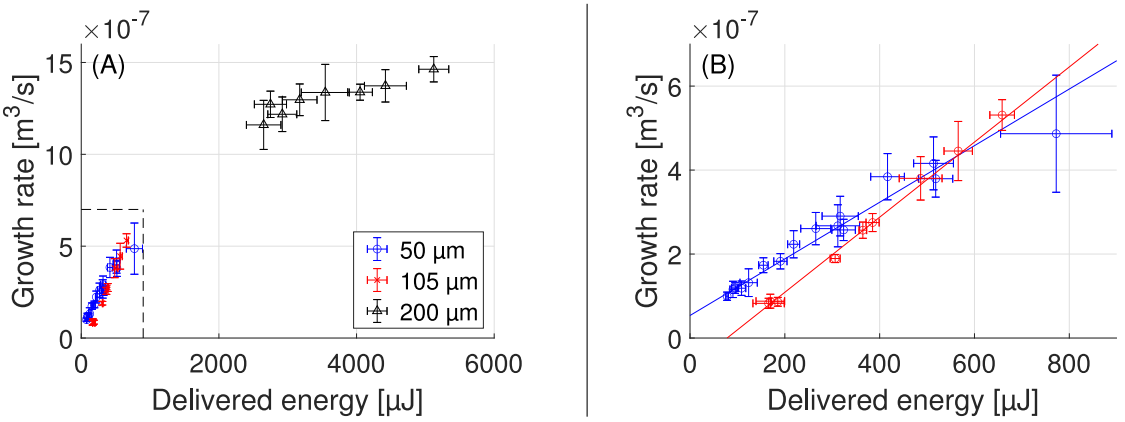

Fig. 9. Average volumetric bubble growth rate for the CW laser. Figure A includes all three fiber sizes. As the energy and growth rates for the 200 µm fiber are much larger compared to the 50 and 105 µm fiber, figure B shows a close-up of the left bottom of (A), indicated by the dotted lines. Figure B includes the best linear fit for the 50 and 105 µm fiber.

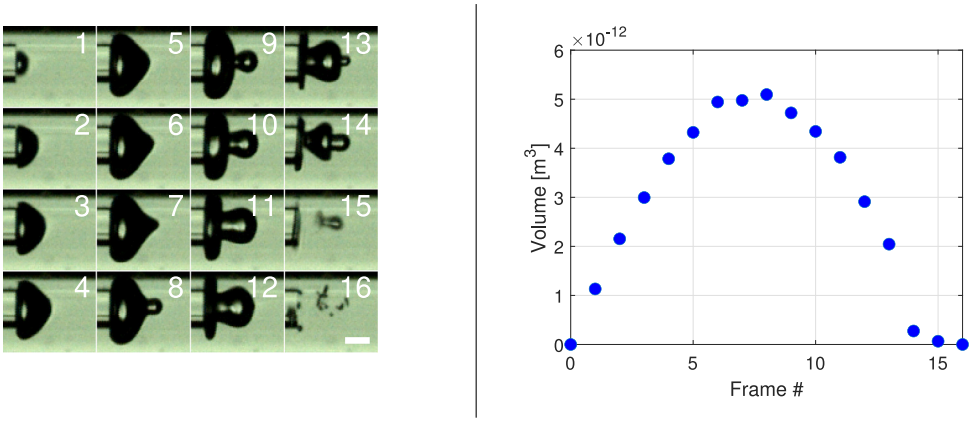

Fig. 10. Left: 16 consecutive frames showing the typical dynamics of a small bubble generated by the CW laser. As the laser is still running during the bubble growth, more liquid will be heated, which results in a secondary (frames 7–12) and even a third bubble (frames 13–14). Snapshots are consecutive, from top to bottom and left to right, with an inter-frame time of 5 µs. The initial nucleation time (top left frame) was 135 µs, and the bubble reached its maximum size (frame 8) at 175 µs. Scalebar on the right bottom measures 100 µm. **Right:** Calculated bubble volume for each frame, showing that the initial maximum is reached at frame 6, but due to secondary bubble formation, another maximum is reached at frame 8, although the difference is small.

The occurrence of these secondary bubbles depends on the laser power and nucleation time of the initial bubble. The secondary bubble forms during the lifetime of the bubble (typically 50–200 µs), during which enough additional energy has to be delivered to form a secondary bubble. We find that these secondary bubbles only appear when the intensities are sufficiently larger such that the initial nucleation time is smaller than approximately 450 µs, both for the 50 and 105 µm fiber. For the 200 µm fiber the intensities are smaller and thus the nucleation times are much larger we did not observe any secondary bubbles. However, we hypothesize that the use of a more powerful laser can also form these secondary bubbles with the 200 µm fiber. However, as mentioned, these secondary bubbles only happen for small nucleation times and large powers, which result in small bubbles overall. Therefore, we conclude that the larger and faster-growing primary bubbles are of more interest.

4.3. Comparison between pulsed and CW

A direct comparison between the bubbles generated by the pulsed and CW laser requires a matching absorption coefficient such that the volumes over which the energy is absorbed are identical. Therefore, we compare the results of the 10 mM ARAC solution, as its absorption coefficient at 532 nm is nearly identical compared to the absorption coefficient of water at 1950 nm. In this subsection, we compare the bubbles generated by the 50 and 105 µm fiber, as they show similar results in the growth rate ($1 - 7 * 10^{-7} m^3/s$). The 200 µm fiber shows very different results for the CW laser, as the delivered energies are much larger (see Fig. 9).

Energy efficiency

The budgeting of energy has practical implications on the right choice of laser source. The growth rates for the CW and pulsed laser are shown in Fig. 11, for the 50 and 105 µm fiber. For the same delivered optical energy, the pulsed laser results in faster growth rates, although the required energies are in the same order of magnitude. Typically, the CW laser requires two to three times more optical energy than the pulsed laser to generate a bubble with the same growth rate. The reduced efficiency is explained by three reasons. First of all, for the bubbles generated by the CW laser heat diffusion cannot be neglected, as the nucleation time is 0.1 - 5 ms, which is in the same order as the thermal diffusion timescale (~ 4 ms, see Eq. (2)). Most of this heat will be lost, as it will heat up the liquid around the irradiated volume. Though this heat increase in the proximate area would be limited, and most of it does not result in the phase transition. Second, the absorption coefficient of water around 1950 nm decreases with increasing temperature, and the absorption coefficient at 100°C is only half the initial value at room temperature [56,57]. Therefore, for the heating phase with the CW laser, the average absorption length is much larger compared to the absorption length of the pulsed laser experiments. Third, for the pulsed laser, there might be non-linear absorption due to

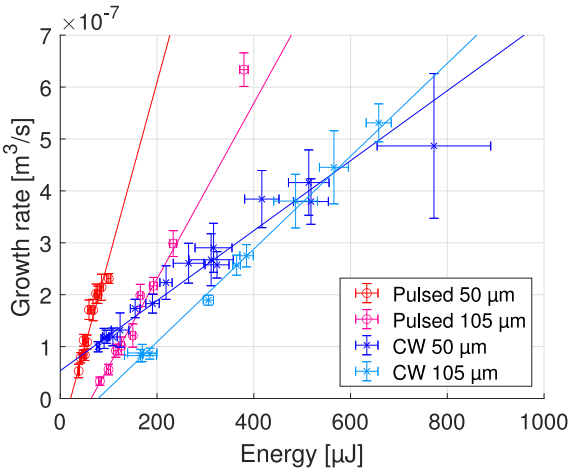

Fig. 11. Growth rate of bubbles generated by the pulsed (red) and CW laser (blue), for fibers with core diameters of 50 (dark colors) and 105 μm (light colors). The absorption coefficients for both lasers are the same ($\alpha \approx 12000$ m^{-1}).

the high peak power. The measured absorption coefficient of the 10 mM ARAC is the same as the absorption coefficient of water for low optical intensities, but the absorption coefficient for the high-power pulses may be larger due to additional non-linear absorption by the liquid. This increased absorption would result in a smaller irradiated volume and thus a higher energy density, which will increase the bubble growth rate.

Bubble dynamics

Bubble dynamics govern the subsequent microfluidic jet parameters. As shown above, the typical growth rates are similar for both lasers. However, identical average growth rates may not result in the exact same bubble characteristics. An increase in growth time, results in a larger bubble, assuming the average growth rate is the same. The maximum volume against the average growth rate is shown in Fig. 12 for the bubbles generated by the pulsed (red) and CW (blue) laser. For identical average growth rates, the bubbles created by the CW laser grow to a ~ 15% larger volume (due to the increased growth time). Alternatively, for bubbles with the same maximum volume, the bubbles created by the CW laser take longer to reach that volume. This reduced growth rate could be explained by the larger volume over which the delivered energy is dissipated, resulting in a less explosive phase transition. However, this also means that for the same average growth rate, the bubbles generated by the CW laser will push out the remaining liquid over a longer length and time. This increased time of energy transfer will mostly affect the jet tail, which is typically slower and more dispersed [16,58]. We hypothesize that this longer growth time results in a faster and more reproducible jet tail.

A comparison between the growth and collapse can be made by normalizing the volume and time, as shown in Fig. 13. For each individual bubble, the volume is normalized by its maximum volume and the time by the growth time. The lines show an average value over all bubbles, and the shaded region is the standard deviation. This figure shows that the initial normalized growth rate of the bubbles generated by the pulsed laser is larger compared to bubbles generated by the CW laser, as indicated by the steeper curve for small times. Furthermore, it shows that for the pulsed laser, the collapse is on average ~ 20% slower compared to the growth, whereas for the CW they take equal time. Both of these findings are in agreement with previous studies on the bubble dynamics for pulsed laser [41,59] and CW [18]. However, this difference is mainly caused by the ~ 15% smaller growth time for the pulsed laser, see Fig. 12. If both curves were normalized by the same time, the time of collapse would only vary by < 5%.

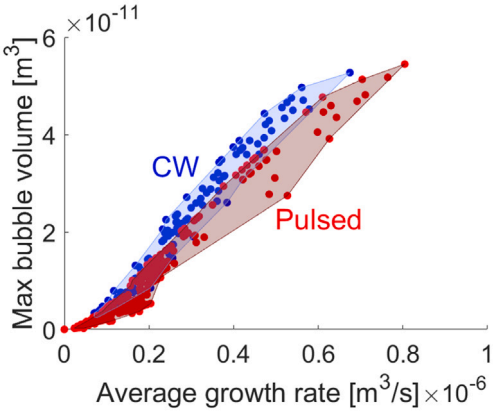

Fig. 12. Maximum bubble volume vs average growth rate for individual bubbles generated by the pulsed laser (red) and the CW laser (blue). The shaded area encapsulates all data.

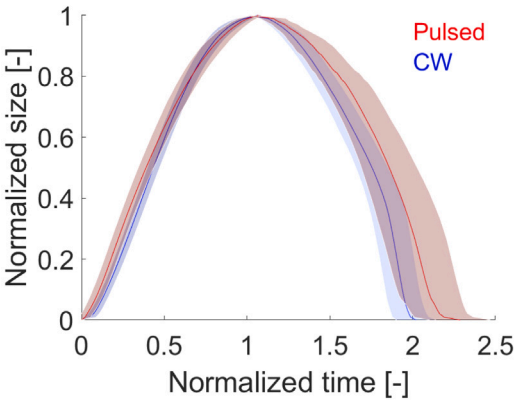

Fig. 13. Normalized bubble size vs normalized time, for CW (blue) and pulsed (red). Lines indicate averages over all bubbles; shaded regions indicate standard deviation. For each individual bubble, the volume is normalized by the maximum volume, and the time is normalized by the growth time.

Reproducibility

Reproducibility is an essential factor considering application in health care. The error bars in Fig. 11 show that the deviation in the bubble growth rate is larger for the CW laser (blue colors) compared to the pulsed laser (red colors). This indicates that even with identical initial conditions for the CW laser, the bubble dynamics can vary each time slightly. As discussed in Section 4.2, the energy delivered by the CW laser is not controlled directly but depends on the laser power and nucleation time. As nucleation is a stochastic event, there is a variance in the nucleation time, resulting in less or more delivered energy for early or late nucleation, respectively.

Fig. 14 shows the growth rate of all individual bubbles generated by the CW laser together with the mean and standard deviation for a group of 6 or more with identical initial conditions (laser power). Each color indicates a different laser power, which influences the delivered energy. However, even for measurements with identical laser power, the delivered energy can vary up to ± 50 μJ. For each laser power, the individual results are typically in the bottom-left or top-right quadrant of the error bars. This indicates a correlation between the additional energy for delayed nucleation and the bubble growth rate. Furthermore, per laser power, the individual data points are fitted with a linear fit, which is shown by the colored lines. The slope of these colored lines is very similar to the slope of the black line, which is the best fit when comprising all data. Therefore, the variance in nucleation time directly affects the bubble growth rate, which means that delayed

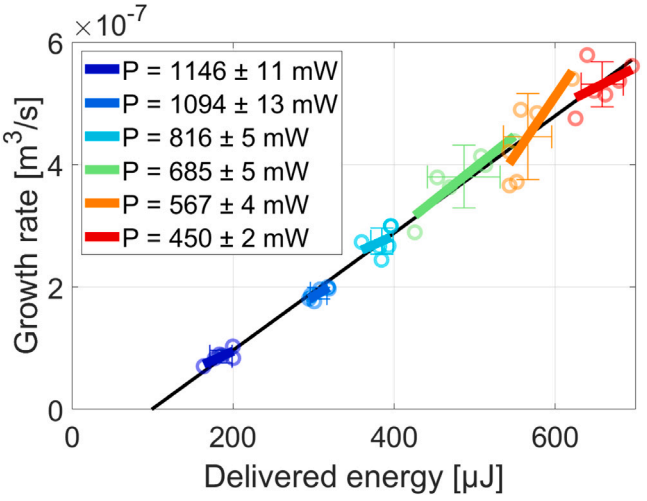

Fig. 14. Growth rate for individual bubble events for the 105 μm fiber with the CW laser. Each color indicates a different laser power. The delivered energy mainly depends on the laser power but also on the moment of nucleation (e.g. late nucleation results in larger delivered energy). The circles are individual measurements, and the error bars indicate the mean and standard deviation of those individual measurements with the same laser power (at least 6). The colored lines indicate the best linear fit per laser power. The black line indicates the best linear fit for all data points. The slope of the colored lines is similar to the black line, indicating a correlation between the nucleation time and the bubble growth rate.

nucleation results in more energy and a faster-growing bubble, and early nucleation results in less energy and a slower-growing bubble. However, as nucleation is a stochastic process, resulting in a random deviation and reducing reproducibility.

For the pulsed laser, the standard deviation in delivered energy is only affected by the laser specifications. On average, it is much smaller with 2% of the delivered energy, compared to 8% for CW. As this deviation also directly affects the bubble growth rate, the bubble growth rate for the pulsed laser is thus more reproducible.

4.4. Practical and future considerations

4.4.1. Laser choice for applications

Engineering a medical device based on laser-induced cavitation is limited by the available offer of laser sources on the market. Yet, choosing the suitable laser emitter is vital for the success of any potential product or prototype, where not only the best physical and optical parameters shall be considered. Other aspects like cost, the robustness of operation, size or compliance with safety hazards play a key role. Intuitively, the cheaper, smaller and safer source is favorable, but these are usually contradictory parameters. The results of this study bring a better understanding of what kind of laser parameters are critical to generating fast-traveling liquid droplets of relevance for its use in eventual devices using laser-induced cavitation, e.g. needle-free jet injectors. Although an in-depth techno-economical discussion on the selection of laser sources for specific applications is beyond the scope of this study, we will briefly discuss the impact of the different laser and device parameters here. The main differences are shown in Table 1.

For applications where reproducibility and reliability of the bubble dynamics are most important, the pulsed laser is preferred over the CW laser. Due to the reduced control over the delivered energy by the CW laser, there is a larger deviation in individual bubble growth rates. In the case of a jet injection device, this affects the jet velocity and, thus, injection depth. However, the exact influence of the deviation in bubble dynamics on the injection depth should be investigated further.

On the other hand, if the device's price and/or size are more important, a CW laser would be preferred over a pulsed laser. Due to their lower power, they are smaller and more affordable. Although, portable pulsed lasers with moderate pulse energies, like those used in our studies, have become more widely available over the past decade.

Furthermore, the use of optical fibers allows for a small handheld device, even in the case of a bulky laser source. The laser source, including electronics, can then be placed in a bench-top part. The choice of optical fiber has a considerable influence on bubble dynamics. For the pulsed laser, a smaller fiber reduces the required pulse energy. However, the smallest fiber (50 μm diameter) is limited in the range of bubble growth rate due to laser-induced damage of the fiber tip. For the CW laser, an increase in fiber size results in faster-growing bubbles, although it requires a more powerful laser (P > 2 W) to create a larger range of growth rates.

Changing the dye concentration has a significant influence on the bubble dynamics. For the pulsed laser, an increase of dye concentration and, thus, absorption coefficient results reduces the required pulse energies, as discussed in Section 4.1. This allows for the use of smaller and more affordable pulsed lasers. Simultaneously, a single device could create a large range of bubbles by changing the absorption coefficient of the liquid. This study has not investigated the influence of the absorption coefficient on the bubbles generated by the CW laser. However, previous studies showed an influence on the nucleation time and bubble size [35,60]. Moreover, adding the dye into drug formulation might bear further toxicity and regulatory issues. Future studies should focus on the exact influence of the absorption coefficient on bubble dynamics.

4.4.2. Comparison with alternative methods for single bubble generation

In this study, a ns-pulsed laser and a low-power CW laser are used for the generation of a single transient bubble. These are the main source for bubble generation for micro-jet injectors [7]. However, there are alternative methods to create reproducible, single transient bubbles: high-voltage discharge [61–63], low-voltage discharge [62], free-running/high-power continuous-wave lasers ($\mathcal{O}$(1 kW)) [30–32] and plasmonic [47,64]. The typical bubble sizes for a range of delivered energies can be seen in Fig. 15. Each point corresponds to a single study, which can be found in Appendix E.

The high-voltage electrical discharge (HVD) requires a large electric field ($\gtrsim 10^6$ V/m) between two electrodes in a liquid environment with low electrical conductivity. This results in electrical breakdown and the formation of a plasma, which reduces the resistance between the electrodes, leading to rapid heating and the formation of a bubble. The bubble size increases with increasing discharge energy [65], electrode distance [62], or decreasing liquid conductivity [62]. Typical bubble sizes are in the order of 0.1–10 mm, with lifetimes of 0.1–5 ms. At the lower end of this range, bubble sizes and lifetimes are very similar to the laser-generated bubbles in this work, and high-power discharge has also already been used for microjet creation [61,63].

For low-voltage discharge (LVD), the two electrodes are in direct contact, for which reason a much lower voltage (~ 50V) is needed for the formation of an electric spark and bubble [66]. Compared to HVD, the discharge event takes much longer [62]. This also results in bubbles with sizes in the range of 1–10 mm and typical lifetimes around 1 ms [62], therefore, LVD results in larger and longer-lived bubbles compared to the laser-generated bubbles in this work. In some cases, the electrodes may break due to large forces during the spark and bubble formation, so the electrodes have to be repositioned for the next bubble formation [66]. Therefore LVD would not be a suitable alternative method.

The free-running Holmium lasers create laser pulses with approximately constant output for 100-1000 μs. Therefore, they may appear to be similar to CW lasers. However, these free-running lasers operate at a much higher power ($\mathcal{O}$(1 kW)) [30–32], and therefore deliver energies in the order of 100–1000 mJ. This results in larger bubbles, which can mainly be used in tissue ablation.

Table 1
Overview of the different laser and bubble characteristics after CW and pulsed laser exposure.

	Pulsed laser	CW laser
Timescale	5 ns	1 ms
Peak power	10^4 W	1 W
Typical price[a]	~1000–50000 $	~100–1000 $
Typical size	Table top device	Handheld device
Control over delivered energy	Direct (input of laser)	Indirect (depends on P & t_n)
Reproducibility (variation)	2%	8%
Ratio growth to collapse time	1:1.2	1:1
Influence of increase in fiber size (laser input parameters constant)	Reduction in energy density Increase in energy threshold Smaller/slower growing bubbles	Delayed nucleation Increase in delivered energy Larger/faster growing bubbles
Influence of increase in absorption coefficient/dye concentration	Larger energy density Decrease in energy threshold Increase of bubble size	Not examined in this study[b]

[a]Laser prices depend highly on wavelength and exact characteristics. Given prices are just an indication of the typical consumer price of a single device.
[b]Refs. [35,60] show that an increase in dye concentration results in shorter nucleation times and smaller bubbles.

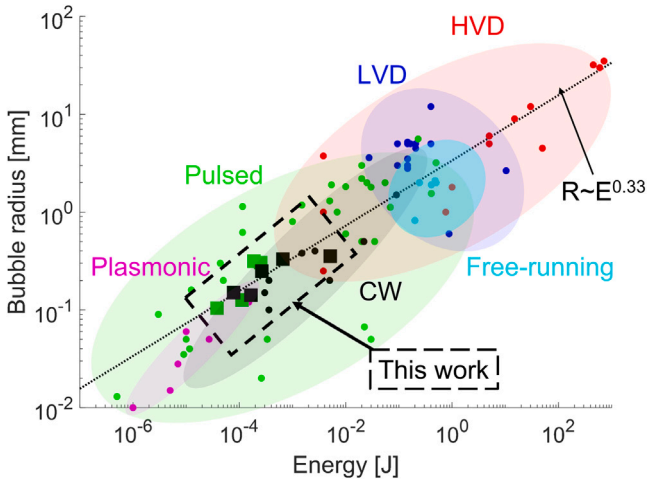

Fig. 15. Comparison of typical bubble sizes and required energies for different methods of single bubble generation. Blue: Low voltage discharge (LVD), Red: High voltage discharge (HVD), Green: Pulsed laser, Black: Low-power Continuous-Wave laser, Cyan: Free-running laser (high-power CW), Magenta: Plasmonic heating. Square symbols indicate typical sizes from current work (low-power CW and pulsed). Each dot is from a different peer-reviewed study, see Appendix E for original references. Part of the data of the voltage discharge and pulsed lasers is taken from tables in Ref. [62]. The black dotted line indicates the best exponential fit with $R\ E^{1/3}$, which indicates that the volume ($V \sim R^3$) is proportional to the delivered energy.

Over the last decade, plasmonic bubbles have received increasing interest [47,64]. Plasmonic nanoparticles absorb CW laser irradiation with high efficiency, quickly heating the surrounding liquid. Due to relatively short nucleation times, the delivered energy remains in the order of 1–100 μJ, resulting in bubble radii smaller than 100 μm. Therefore, these have not yet been used for microjet formation.

4.4.3. Recommendations for future developments

Our study was mainly experimental and thus has some limitations. Here, we discuss such limitations and suggest further studies to improve the understanding and application of laser-generated bubbles.

- We studied bubbles in single cylindrical confinement with a fixed liquid filling level. This confinement was chosen because we used it in previous jet injection studies [16,45]. However, different confinements have been reported, such as moon-shaped channels [18], or channels including a tapered nozzle [19] and/or a membrane [67]. A change in confinement will affect the bubble dynamics; however, we hypothesize that this would have similar effects on both CW and pulsed-laser-generated bubbles. Therefore, our results presented here are a representative comparison.
- The liquid we used in our experiments is (dyed) water with low viscosity. This allows for easy comparison with further academic studies. However, in practical applications, additional drug formulation or different inks may affect the viscosity or elasticity and therefore, the bubble and jet dynamics [68]. We consider that careful parametric studies exploring different liquid properties will be crucial to enable the use of cavitation in the development of real-life applications.
- In the case of small bubbles ($R < 25$ μm or $\tau < 40$ μs), the spatial and temporal imaging resolution of the tracking of the bubble size and lifetime are less accurate. This spatiotemporal resolution was chosen as it captures a wide range of bubble dynamics, from inception/nucleation, growth and collapse. However, the inaccuracy of tracking small bubbles may result in an error in the calculated energy threshold for bubble formation. Further studies focusing on this threshold should use an increased spatiotemporal resolution to image the smallest bubbles. Moreover, a larger range of fiber sizes and absorption coefficients may improve the understanding of this threshold.
- This study has been predominantly experimental and focused on the medical application of the bubbles in jet injectors. Therefore, other relevant theoretical aspects were not studied and more work is needed to fully understand laser-driven cavitation. Numerical simulations could help in gaining more understanding, but this may remain challenging because the influence of a few parameters remains unknown. Firstly, due to the spatiotemporal imaging resolution limitation of our microscopes and high-speed cameras, very small bubbles near the threshold are less accurate. Comparing these with a model will presumably include a large error. Secondly, the effects of the wall, including heat transfer and viscous friction, are complex and not fully understood.

5. Conclusion

We experimentally compared the dynamics of bubbles generated by two lasers with different timescales (ns and ms) inside an open-ended capillary filled with liquid. Our comparative study is the first to show the resulting bubble dynamics in the same fluidic confinement with two different laser types. We have shown that these lasers create bubbles of comparable growth rates proportional to the delivered energy. This linear increase agrees with the previously found proportionality between the energy and the jet velocity.

For the pulsed laser set-up, we found that the energy threshold for nucleation is proportional to the irradiated volume. This volume depends on the fiber core radius, beam divergence and absorption

coefficient. Therefore, a decrease in irradiated volume, either by changing the fiber or increasing the absorption coefficient, reduces the energy threshold. This allows for the use of more affordable and/or less powerful pulsed laser sources while creating the same bubble characteristics.

For the continuous-wave laser, we found an efficiency increase and better reproducibility compared to previous experiments with free-space optics. This is explained by a reduction in the number of interfaces and easier alignment. Furthermore, we show that the delivered energy can be controlled by the laser power and the fiber size. For each fiber, a decrease in laser power results in an increase in delivered energy, allowing the creation of faster-growing bubbles. Furthermore, a larger fiber results in an increase in delivered energy for fixed laser powers due to a longer nucleation time. Therefore, the 200 μm fiber results in much larger and faster-growing bubbles than the 50 or 105 μm fiber, when the same laser power is used.

The comparison between the two laser sources shows that the pulsed laser requires slightly less optical energy to create the same bubble growth rate, which we attribute to heat dissipation and a reduction in absorption coefficient during the CW laser heating. However, for the same average growth rate, bubbles generated by the CW laser grow for a longer time and are larger.

Finally, we compared both methods in terms of practical usage. Since the delivered energy by the CW laser cannot be controlled directly, there is a larger deviation in the delivered energy compared to the pulsed lasers (8% and 2%, respectively), which also results in a more significant deviation in bubble growth rates. This would be unfavorable for laser-based jet injection, as it decreases the control over jet velocity and, therefore, injection depth. However, if this variation is within the allowable error industry standards, then the CW laser could be advantageous due to its smaller size and lower price compared to pulsed lasers.

CRediT authorship contribution statement

Jelle J. Schoppink: Conceptualization, Methodology, Formal analysis, Investigation, Data curation, Writing – original draft, Visualization. **Jan Krizek:** Conceptualization, Methodology, Writing – review & editing. **Christophe Moser:** Conceptualization, Funding acquisition, Writing – review & editing. **David Fernandez Rivas:** Conceptualization, Supervision, Project administration, Funding acquisition, Writing – review & editing.

Declaration of competing interest

The authors declare the following financial interests/personal relationships which may be considered as potential competing interests: David Fernandez Rivas reports financial support was provided by European Research Council. David Fernandez Rivas reports financial support was provided by Ministry of Education, Culture and Science of the Government of the Netherlands. Jan Krizek & Christophe Moser reports financial support was provided by Innosuisse Swiss Innovation Agency. Jelle Schoppink reports financial support was provided by European Research Council. Jelle Schoppink reports financial support was provided by Ministry of Education, Culture and Science of the Government of the Netherlands. David Fernandez Rivas has patent pending to University of Twente. Jan Krizek & Christophe Moser has patent pending to ECOLE POLYTECHNIQUE FED LAUSANNE EPFL. Co-founder of FlowBeams, a spin-off company of the University of Twente on needle-free injection, David Fernandez Rivas.

Data availability

Data will be made available on request

Acknowledgments

J.J.S. would like to thank dr. Daniël Jáuregui-Vázquez, dr. Jose Alvarez Chavez and Frans Segerink for their help with the optical set-up of the CW laser and K. Mohan for her help with surface tension and viscosity measurements. J.J.S and D.F.R. acknowledge the funding from the European Research Council (ERC) under the European Union's Horizon 2020 Research and Innovation Programme (Grant Agreement No. 851630), and NWO Take-off phase 1 program funded by the Ministry of Education, Culture and Science of the Government of the Netherlands (No. 18844). J.K. and Ch.M. acknowledge the Innosuisse BRIDGE Proof of Concept grant funding. The authors are thankful for the insightful discussions with Dr. M. A. Quetzeri Santiago, D.L. van der Ven, K. Mohan and D. de Boer.

Appendix A. Supplementary data

Supplementary material related to this article can be found online at https://doi.org/10.1016/j.expthermflusci.2023.110926.

References

[1] Qian Peng, Asta Juzeniene, Jiyao Chen, Lars O. Svaasand, Trond Warloe, Karl Erik Giercksky, Johan Moan, Lasers in medicine, Rep. Progr. Phys. (ISSN: 00344885) 71 (5) (2008) http://dx.doi.org/10.1088/0034-4885/71/5/056701.

[2] Alfred Vogel, Vasan Venugopalan, Mechanisms of pulsed laser ablation of biological tissues, Chem. Rev. (ISSN: 00092665) 103 (2) (2003) 577–644, http://dx.doi.org/10.1021/cr010379n.

[3] Shubho Mohajan, Jean Christophe Delagnes, Baptiste Allisy, Antonio Iazzolino, Bertrand Viellerobe, Stéphane Petit, Plasma-free bubble cavitation in water by a 2.9 μ m laser for bioprinting applications, Appl. Phys. Lett. (ISSN: 00036951) 121 (24) (2022) http://dx.doi.org/10.1063/5.0126355.

[4] Séverine Le Gac, Ed Zwaan, Albert Van Den Berg, Claus Dieter Ohl, Sonoporation of suspension cells with a single cavitation bubble in a microfluidic confinement, Lab on A Chip (ISSN: 14730189) 7 (12) (2007) 1666–1672, http://dx.doi.org/10.1039/b712897p.

[5] Nathaniel M. Fried, Recent advances in infrared laser lithotripsy [Invited], Biomed. Optics Express (ISSN: 2156-7085) 9 (9) (2018) 4552, http://dx.doi.org/10.1364/boe.9.004552.

[6] Andrew J. Marks, Joel M.H. Teichman, Lasers in clinical urology: State of the art and new horizons, World J. Urol. (ISSN: 07244983) 25 (3) (2007) 227–233, http://dx.doi.org/10.1007/s00345-007-0163-x.

[7] Jelle Schoppink, David Fernandez Rivas, Jet injectors: Perspectives for small volume delivery with lasers, Adv. Drug Deliv. Rev. (ISSN: 18728294) 182 (2022) 114109, http://dx.doi.org/10.1016/j.addr.2021.114109.

[8] Catherine Daly, Natalia A. Molodecky, Meghana Sreevatsava, Asalif D. Belayneh, Shoukat A. Chandio, Jeff Partridge, Ahmed Shaikh, Mumtaz Laghari, John Agbor, Rana M. Safdar, Umar Farooq Bullo, Safi M. Malik, Abdirahman Mahamud, Needle-free injectors for mass administration of fractional dose inactivated poliovirus vaccine in Karachi, Pakistan: A survey of caregiver and vaccinator acceptability, Vaccine (ISSN: 18732518) 38 (8) (2020) 1893–1898, http://dx.doi.org/10.1016/j.vaccine.2019.12.059.

[9] Samir S. Mitragotri, Immunization without needles, Nat. Rev. Immunol. (ISSN: 14741733) 5 (12) (2005) 905–916, http://dx.doi.org/10.1038/nri1728.

[10] Samir S. Mitragotri, Current status and future prospects of needle-free liquid jet injectors, Nat. Rev. Drug Discov. (ISSN: 14741776) 5 (7) (2006) 543–548, http://dx.doi.org/10.1038/nrd2076.

[11] Rhys Matthew James Williams, Bryan P. Ruddy, N. Catherine Hogan, Ian W. Hunter, Poul M.F. Nielsen, Andrew J. Taberner, Analysis of moving-coil actuator jet injectors for viscous fluids, IEEE Trans. Biomed. Eng. (ISSN: 15582531) 63 (6) (2016) 1099–1106, http://dx.doi.org/10.1109/TBME.2015.2482967.

[12] James W. McKeage, Bryan P. Ruddy, Poul M.F. Nielsen, Andrew J. Taberner, The effect of jet speed on large volume jet injection, J. Control. Release (ISSN: 18734995) 280 (September 2017) (2018) 51–57, http://dx.doi.org/10.1016/j.jconrel.2018.04.054.

[13] Pol Sopeña, Javier Arrese, Sergio González-Torres, Juan Marcos Fernández-Pradas, Albert Cirera, Pere Serra, Low-cost fabrication of printed electronics devices through continuous wave laser-induced forward transfer, ACS Appl. Mater. Interfaces (ISSN: 19448252) 9 (35) (2017) 29412–29417, http://dx.doi.org/10.1021/acsami.7b04409.

[14] Moliria V. Santos, Kelly T. Paula, Marcelo B. De Andrade, Emmanuel M. Gomes, Lippy F. Marques, Sidney J.L. Ribeiro, Cleber R. Mendonça, Direct femtosecond laser printing of silk fibroin microstructures, ACS Appl. Mater. Interfaces (ISSN: 19448252) 12 (44) (2020) 50033–50038, http://dx.doi.org/10.1021/acsami.0c13482.

[15] Yoshiyuki Tagawa, Nikolai Oudalov, Claas Willem Visser, Ivo R. Peters, Devaraj van der Meer, Chao Sun, Andrea Prosperetti, Detlef Lohse, Highly focused supersonic microjets, Phys. Rev. X (ISSN: 21603308) 2 (3) (2012) http://dx.doi.org/10.1103/PhysRevX.2.031002.

[16] Jan Krizek, Frédéric De Goumoëns, Paul Delrot, Christophe Moser, Needle-free delivery of fluids from compact laser- based jet injector, Lab on A Chip (20) (2020) 3784–3791, http://dx.doi.org/10.1039/d0lc00646g.

[17] C. Berrospe-Rodriguez, Claas Willem Visser, Stefan Schlautmann, Ruben Ramos-Garcia, David Fernandez Rivas, Continuous-wave laser generated jets for needle free applications, Biomicrofluidics (ISSN: 19321058) 10 (2016) http://dx.doi.org/10.1063/1.4940038.

[18] Loreto Oyarte Gálvez, Arjan Fraters, Herman L. Offerhaus, Michel Versluis, Ian W. Hunter, David Fernández Rivas, Microfluidics control the ballistic energy of thermocavitation liquid jets for needle-free injections, J. Appl. Phys. (ISSN: 0021-8979) (2020) http://dx.doi.org/10.1063/1.5140264.

[19] Diana L. van der Ven, Davide Morrone, Miguel A. Quetzeri-Santiago, David Fernandez Rivas, Microfluidic jet impact: spreading, splashing, soft substrate deformation and injection, J. Colloid Interface Sci. (2023) http://dx.doi.org/10.1016/j.jcis.2023.01.024, arXiv:2207.12167.

[20] Hwi Chan Ham, Hun Jae Jang, Jack J. Yoh, A check valve controlled laser-induced microjet for uniform transdermal drug delivery, AIP Adv. (ISSN: 21583226) 7 (12) (2017) 125206, http://dx.doi.org/10.1063/1.4999962.

[21] V. Robles, E Gutierrez-Herrera, Luis Felipe Devia-Cruz, D. Banks, S. Camacho-Lopez, Guillermo Aguilar, Soft material perforation via double-bubble laser-induced cavitation microjets soft material perforation via double-bubble laser-induced cavitation microjets, Phys. Fluids 32 (042005) (2020) http://dx.doi.org/10.1063/5.0007164.

[22] Pankaj Rohilla, Jeremy O. Marston, Feasibility of laser induced jets in needle free jet injections, Int. J. Pharm. (ISSN: 03785173) (2020) 119714, http://dx.doi.org/10.1016/j.ijpharm.2020.119714.

[23] Yoshiyuki Tagawa, Nikolai Oudalov, A. El Ghalbzouri, Chao Sun, Detlef Lohse, Needle-free injection into skin and soft matter with highly focused microjets, Lab on A Chip (ISSN: 14730189) (2013) http://dx.doi.org/10.1039/c2lc41204g.

[24] Carla Berrospe-Rodriguez, Claas Willem Visser, Stefan Schlautmann, David Fernandez Rivas, Ruben Ramos-Garcia, Toward jet injection by continuous-wave laser cavitation, J. Biomed. Opt. (ISSN: 1560-2281) (2017) http://dx.doi.org/10.1117/1.jbo.22.10.105003.

[25] Miguel A. Quetzeri-Santiago, Ian W. Hunter, Devaraj van der Meer, David Fernandez Rivas, Impact of a microfluidic jet on a pendant droplet, Soft Matter (ISSN: 1744-683X) (2021) 1–18, http://dx.doi.org/10.1039/d1sm00706h.

[26] Alfred Vogel, J. Noack, K. Nahen, D. Theisen, S. Busch, U. Parlitz, D.X. Hammer, G.D. Noojin, B.A. Rockwell, R. Birngruber, Energy balance of optical breakdown in water at nanosecond to femtosecond time scales, Appl. Phys. B (ISSN: 09462171) (1999) http://dx.doi.org/10.1007/s003400050617.

[27] Emil Alexandru Brujan, Kester Nahen, Peter Schmidt, Alfred Vogel, Dynamics of laser-induced cavitation bubbles near an elastic boundary, J. Fluid Mech. (ISSN: 00221120) 433 (2001) 251–281, http://dx.doi.org/10.1017/S0022112000003347.

[28] A. Vogel, S. Busch, U. Parlitz, Shock wave emission and cavitation bubble generation by picosecond and nanosecond optical breakdown in water, J. Acoust. Soc. Am. (ISSN: 0001-4966) 100 (1) (1996) 148–165, http://dx.doi.org/10.1121/1.415878.

[29] Emil Alexandru Brujan, Alfred Vogel, Stress wave emission and cavitation bubble dynamics by nanosecond optical breakdown in a tissue phantom, J. Fluid Mech. (ISSN: 14697645) 558 (2006) 281–308, http://dx.doi.org/10.1017/S0022112006000115,

[30] Thomas Asshauer, K. Rink, Guy P. Delacretaz, Acoustic transient generation by holmium-laser-induced cavitation bubbles, J. Appl. Phys. (ISSN: 00218979) 76 (9) (1994) 5007–5013, http://dx.doi.org/10.1063/1.357212.

[31] Thomas Asshauer, Thomas Jansen, Thorsten Oberthur, Guy P. Delacretaz, Bruno E. Gerber, Holmium laser ablation of cartilage: effects of cavitation bubbles, in: Laser-Tissue Interaction VI, Vol. 2391, no. May 1995, (ISSN: 1996756X) 1995, p. 379, http://dx.doi.org/10.1117/12.209905.

[32] Thomas Asshauer, Guy P. Delacretaz, E.D. Jansen, A.J. Welch, M. Frenz, Pulsed holmium laser ablation of tissue phantoms: Correlation between bubble formation and acoustic transients, Appl. Phys. B (ISSN: 09462171) 65 (4–5) (1997) 647–657, http://dx.doi.org/10.1007/s003400050327.

[33] Michael Ith, Martin Frenz, Hans S. Pratisto, Heinz P. Weber, Hans J. Altermatt, Hans U. Staeubli, Thomas Asshauer, Guy P. Delacretaz, Rene-Paul Salathe, Bruno E. Gerber, Influence of pulse duration on erbium and holmium laser ablation under water, in: Laser Interaction with Hard and Soft Tissue II, Vol. 2323, no. January 1995, ISBN: 0819416568, 1995, pp. 130–138, http://dx.doi.org/10.1117/12.199190.

[34] J.P. Padilla-Martinez, C. Berrospe-Rodriguez, Guillermo Aguilar, J.C. Ramirez-San-Juan, Ruben Ramos-Garcia, Optic cavitation with CW lasers: A review, Phys. Fluids (ISSN: 10897666) 26 (12) (2014) http://dx.doi.org/10.1063/1.4904718.

[35] Bin Zhang, Darren Banks, Vicente Robles, Luis Felipe, Devia Cruz, Guillermo Aguilar, High resolution optical investigation of laser intensity and solution temperature effects on thermocavitation, Exp. Therm Fluid Sci. (ISSN: 0894-1777) 136 (April) (2022) 110683, http://dx.doi.org/10.1016/j.expthermflusci.2022.110683.

[36] S.M. Afanador-Delgado, R. Sevilla-Escoboza, V.F. Marañón-Ruíz, R. Chiu, Influence of the anthocyanin concentration in ethanolic extracts of Hibiscus Sabdariffa on thermocavitation: An analysis of the pulse frequency and amplitude, Opt. Laser Technol. (ISSN: 00303992) 132 (2020) http://dx.doi.org/10.1016/j.optlastec.2020.106468.

[37] J.P. Padilla-Martinez, Guillermo Aguilar, J.C. Ramirez-San-Juan, Ruben Ramos-Garcia, Temporal evolution of thermocavitation bubbles using high speed video camera, in: Optical Trapping and Optical Micromanipulation VIII, Vol. 8097, no. September 2011, (ISSN: 0277786X) ISBN: 9780819487070, 2011, 809727, http://dx.doi.org/10.1117/12.894467.

[38] Steven L. Jacques, Role of tissue optics and pulse duration on tissue effects during high-power laser irradiation, Appl. Opt. (ISSN: 0003-6935) 32 (13) (1993) 2447, http://dx.doi.org/10.1364/ao.32.002447.

[39] Ruru Deng, Yingqing He, Yan Qin, Qidong Chen, Lei Chen, Measuring pure water absorption coefficient in the near-infrared spectrum (900 — 2500 nm), J. Remote Sens. 16 (1) (2012) 192–206.

[40] Günther Paltauf, Peter E. Dyer, Photomechanical processes and effects in ablation, Chem. Rev. (ISSN: 00092665) 103 (2) (2003) 487–518, http://dx.doi.org/10.1021/cr010436c.

[41] Chao Sun, Edip Can, Rory Dijkink, Detlef Lohse, Andrea Prosperetti, Growth and collapse of a vapour bubble in a microtube: The role of thermal effects, J. Fluid Mech. (ISSN: 00221120) 632 (2009) 5–16, http://dx.doi.org/10.1017/S0022112009007381.

[42] G. Paltauf, H. Schmidt-Kloiber, M. Frenz, Photoacoustic waves excited in liquids by fiber-transmitted laser pulses, J. Acoust. Soc. Am. (ISSN: 0001-4966) 104 (2) (1998) 890–897, http://dx.doi.org/10.1121/1.423334.

[43] M. Frenz, G. Paltauf, H. Schmidt-Kloiber, Laser-generated cavitation in absorbing liquid induced by acoustic diffraction, Phys. Rev. Lett. (ISSN: 10797114) 76 (19) (1996) 3546–3549, http://dx.doi.org/10.1103/PhysRevLett.76.3546.

[44] A. Daerr, A. Mogne, Pendent_Drop: An imagej plugin to measure the surface tension from an image of a pendent drop, J. Open Res. Softw. 4 (1) (2016) http://dx.doi.org/10.5334/jors.97.

[45] Jan Krizek, Paul Delrot, Christophe Moser, Repetitive regime of highly focused liquid microjets for needle-free injection, Sci. Rep. (ISSN: 20452322) (2020) http://dx.doi.org/10.1038/s41598-020-61924-0.

[46] Keisuke Hayasaka, Akihito Kiyama, Yoshiyuki Tagawa, Effects of pressure impulse and peak pressure of a shockwave on microjet velocity in a microchannel, Microfluid. Nanofluid. (ISSN: 16134990) (2017) http://dx.doi.org/10.1007/s10404-017-2004-6.

[47] Zhenhong Wang, Bin Zhang, Jun Liu, Yufeng Song, Han Zhang, Recent developments in mid-infrared fiber lasers: Status and challenges, Opt. Laser Technol. (ISSN: 00303992) 132 (July) (2020) 106497, http://dx.doi.org/10.1016/j.optlastec.2020.106497.

[48] Mi Ae Park, Hun Jae Jang, Fedir V. Sirotkin, Jack J. Yoh, Er:YAG laser pulse for small-dose splashback-free microjet transdermal drug delivery, Opt. Lett. (ISSN: 0146-9592) 37 (18) (2012) 3894, http://dx.doi.org/10.1364/ol.37.003894.

[49] Hun Jae Jang, Mi Ae Park, Fedir V. Sirotkin, Jack J. Yoh, Laser-induced microjet: Wavelength and pulse duration effects on bubble and jet generation for drug injection, Appl. Phys. B (ISSN: 09462171) 113 (3) (2013) 417–421, http://dx.doi.org/10.1007/s00340-013-5479-1.

[50] George M. Hale, Marvin R. Querry, Optical constants of water in the 200-nm to 200-μm wavelength region, Appl. Opt. (ISSN: 00036935) 12 (3) (1973) 555, http://dx.doi.org/10.1364/ao.12.000555.

[51] Hun Jae Jang, Seonggu Yeo, Jack J. Yoh, Synchronization of skin ablation and microjet injection for an effective transdermal drug delivery, Appl. Phys. A (ISSN: 1432-0630) 122 (4) (2016) 1–8, http://dx.doi.org/10.1007/s00339-016-9941-x.

[52] Jan Krizek, Barbora Lavickova, Christophe Moser, Degradation study on molecules released from laser-based jet injector, Int. J. Pharm. (ISSN: 18733476) 602 (2021) 120664, http://dx.doi.org/10.1016/j.ijpharm.2021.120664.

[53] Pedro A. Quinto-Su, Madoka Suzuki, Claus-Dieter Ohl, Fast temperature measurement following single laser-induced cavitation inside a microfluidic gap, Sci. Rep. (ISSN: 20452322) (2014) http://dx.doi.org/10.1038/srep05445.

[54] P. Koukouvinis, M. Gavaises, O. Supponen, M. Farhat, Simulation of bubble expansion and collapse in the vicinity of a free surface, Phys. Fluids (ISSN: 10897666) 28 (5) (2016) http://dx.doi.org/10.1063/1.4949354.

[55] Nikolaos Kyriazis, Phoevos Koukouvinis, Manolis Gavaises, Numerical investigations on bubble-induced jetting and shock wave focusing: Application on a needle-free injection, Proc. R. Soc. A (ISSN: 14712946) (2019) http://dx.doi.org/10.1098/rspa.2018.0548.

[56] E. Duco Jansen, Ton G. van Leeuwen, Massoud Motamedi, Cornelius Borst, Ashley J. Welch, Temperature dependence of the absorption coefficient of water for midinfrared laser radiation, Lasers Surg. Med. (ISSN: 10969101) 14 (3) (1994) 258–268, http://dx.doi.org/10.1002/lsm.1900140308.

[57] Björn I. Lange, Tobias Brendel, Gereon Hüttmann, Temperature dependence of light absorption in water at holmium and thulium laser wavelengths, Appl. Opt. (ISSN: 0003-6935) 41 (27) (2002) 5797, http://dx.doi.org/10.1364/ao.41.005797.

[58] Jelle J. Schoppink, Keerthana Mohan, Miguel A. Quetzeri-Santiago, Gareth McKinley, David Fernandez Rivas, Andrew K. Dickerson, Cavitation-induced microjets tuned by channels with alternating wettability patterns, Phys. Fluids 35 (032017) (2023) http://dx.doi.org/10.1063/5.0143223.

[59] Ed Zwaan, Séverine Le Gac, Kinko Tsuji, Claus-Dieter Ohl, Controlled cavitation in microfluidic systems, Phys. Rev. Lett. (ISSN: 00319007) (2007) http://dx.doi.org/10.1103/PhysRevLett.98.254501.

[60] Samuel M. Afanador Delgado, José O. García Medel, Virginia Marañón Ruíz, Ricardo Sevilla Escoboza, Roger Chiu, Solvent effect in extra-cavity pulses by thermo-cavitation in natural dyes, in: SPIE LASE, 2019, no. March 2019, (ISSN: 1996756X) ISBN: 9781510624481, 2019, p. 21, http://dx.doi.org/10.1117/12.2507054.

[61] Daniel A. Fletcher, D.V. Palanker, Pulsed liquid microjet for microsurgery, Appl. Phys. Lett. (ISSN: 00036951) 78 (13) (2001) 1933–1935, http://dx.doi.org/10.1063/1.1357452.

[62] Darjan Podbevšek, Žiga Lokar, Jure Podobnikar, Rok Petkovšek, Matevž Dular, Experimental evaluation of methodologies for single transient cavitation bubble generation in liquids, Exp. Fluids (ISSN: 14321114) 62 (8) (2021) 1–28, http://dx.doi.org/10.1007/s00348-021-03260-1,

[63] Hwichan Ham, Jack J. Yoh, A liquid breakdown driven non-invasive microjet injection system, Med. Eng. Phys. (ISSN: 13504533) 92 (2021) 54–63, http://dx.doi.org/10.1016/j.medengphy.2021.05.002.

[64] Mikhail E. Zaytsev, Guillaume Lajoinie, Yuliang Wang, Detlef Lohse, Harold J.W. Zandvliet, Xuehua Zhang, Plasmonic bubbles in n-alkanes, J. Phys. Chem. C (ISSN: 19327455) 122 (49) (2018) 28375–28381, http://dx.doi.org/10.1021/acs.jpcc.8b09617, arXiv:1903.11553.

[65] Yifan Huang, Hui Yan, Bingzhe Wang, Xuming Zhang, Zhen Liu, Keping Yan, The electro-acoustic transition process of pulsed corona discharge in conductive water, J. Phys. D: Appl. Phys. (ISSN: 13616463) 47 (25) (2014) http://dx.doi.org/10.1088/0022-3727/47/25/255204.

[66] Kelly Siew Fong Lew, Evert Klaseboer, Boo Cheong Khoo, A collapsing bubble-induced micropump: An experimental study, Sensors Actuators A (ISSN: 09244247) 133 (1) (2007) 161–172, http://dx.doi.org/10.1016/j.sna.2006.03.023.

[67] Tae Hee Han, Jack J. Yoh, A laser based reusable microjet injector for transdermal drug delivery, J. Appl. Phys. (ISSN: 00218979) (2010) http://dx.doi.org/10.1063/1.3430989.

[68] A. Franco-Gómez, H. Onuki, Y. Yokoyama, Y. Nagatsu, Yoshiyuki Tagawa, Effect of liquid elasticity on the behaviour of high-speed focused jets, Exp. Fluids (ISSN: 0723-4864) 62 (2) (2021) 1–15, http://dx.doi.org/10.1007/s00348-020-03128-w,